



HAL
open science

Evaluation of Scatterer Parameters From Ultrasound Scattering Models Taking Into Account Scattering From Nuclei and Cells of Cell-Pellet Biophantoms and Ex Vivo Tumors

Pauline Muleki-Seya, William D O'Brien

► **To cite this version:**

Pauline Muleki-Seya, William D O'Brien. Evaluation of Scatterer Parameters From Ultrasound Scattering Models Taking Into Account Scattering From Nuclei and Cells of Cell-Pellet Biophantoms and Ex Vivo Tumors. Ultrasonic Imaging, In press, 10.1177/01617346241256120 . hal-04612237

HAL Id: hal-04612237

<https://hal.science/hal-04612237>

Submitted on 14 Jun 2024

HAL is a multi-disciplinary open access archive for the deposit and dissemination of scientific research documents, whether they are published or not. The documents may come from teaching and research institutions in France or abroad, or from public or private research centers.

L'archive ouverte pluridisciplinaire **HAL**, est destinée au dépôt et à la diffusion de documents scientifiques de niveau recherche, publiés ou non, émanant des établissements d'enseignement et de recherche français ou étrangers, des laboratoires publics ou privés.

Evaluation of scatterer parameters from ultrasound scattering models taking into account scattering from nuclei and cells of cell-pellet biophantoms and *ex vivo* tumors

Journal Title
XX(X):2-16
©The Author(s) 2016
Reprints and permission:
sagepub.co.uk/journalsPermissions.nav
DOI: 10.1177/ToBeAssigned
www.sagepub.com/

SAGE

Pauline Muleki-Seya¹ and William D. O'Brien, Jr.²

Abstract

The Quantitative Ultrasound backscatter coefficient provides the capability to evaluate tissue microstructure parameters. Tissue-based scatterer parameters are extracted using ultrasound scattering models. It is challenging to correlate ultrasound scatterer parameters of tissue structures from optical-measured histology, possibly because of inappropriate scattering models or the presence of multiple scatterers. The objective of this study is to pursue the quantification of pertinent scatterer parameters with scattering models that consider ultrasound scattering from nuclei and cells. The concentric sphere model (CSM) and the structure factor model adapted for two types of scatterers (SFM2) are evaluated for cell-pellet biophantoms and *ex vivo* tumors of 4 cell lines: 4T1, JC, LMTK and MAT. The structure factor model (SFM) was used for comparison. CSM and SFM2 provided scatterer parameters closer to histology (lower relative errors) for nucleus and cell radii and volume fractions than SFM but were not always accompanied by lower dispersion of the scatterer distribution (lower coefficient of variation). CSM and SFM2 quantified cell and nucleus radius and volume fraction parameters with lower relative error compared to SFM. For tumors, CSM provided better results than SFM2.

Keywords

Backscatter coefficient, Cell-pellet biophantoms, Scatterer parameters, Structure Factor Model, Concentric Sphere Model

Introduction

The Quantitative Ultrasound (QUS) backscatter coefficient (BSC) contains inherent properties of tissue microstructure. This type of tissue information is valuable when tissue microstructure is affected, for example, in the presence of fat droplets in the liver for nonalcoholic fatty liver disease patients [Lin et al. \(2015\)](#); [Wu et al. \(2020\)](#); [Han et al. \(2020\)](#), cell-death changes (condensation and fragmentation of nuclei and cells via apoptosis) during anti-cancer therapy [Kolios et al. \(2002\)](#), tissue/tumor alteration during high-intensity focused ultrasound heating treatment [Kemmerer et al. \(2013\)](#), and comparison between cancerous and healthy tissues [Mamou et al. \(2011\)](#).

An inverse problem approach was used to quantify ultrasound scatterer parameters from BSC such as the scatterer radius and the acoustic concentration when the Gaussian model or the fluid-filled sphere model is used [Insana et al. \(1993\)](#). However, it is generally difficult to correlate the QUS-measured scatterer parameters with tissue structures derived from optical-measured histology [Oelze and O'Brien Jr. \(2006\)](#); [Muleki-Seya et al. \(2016\)](#). These models deal with identical randomly and independently distributed scatterers, making them valid only for low-concentration (volume fraction <3%) media. Thus, challenges result because tissue is not necessarily considered

ultrasonically a low-concentration media.

The structure factor model (SFM) [Twersky \(1987\)](#); [Franceschini and Guillermin \(2012\)](#), combining incoherent and coherent BSC contributions, is adapted for concentrated (volume fraction >9%) media. Using the SFM, it is possible to quantify scatterer radius, its volume fraction and its relative impedance contrast. In a previous study, the use of the SFM yielded ultrasound-derived scatterer parameters close to histology-derived cellular structures: nuclei for canine liver (with a relative error in radius and volume fraction <7%) and whole cells for HT29 tumors (with a relative error in radius and volume fraction <15%) [Muleki-Seya et al. \(2016\)](#). In another SFM study [Muleki-Seya and O'Brien Jr. \(2022\)](#), the mean relative errors of scatterer radius and volume fraction were <14% (17%, respectively) for LMTK (MAT, respectively) cell-pellet (CP) biophantoms

¹Univ Lyon, INSA-Lyon, Université Claude Bernard Lyon 1, UJM-Saint Etienne, CNRS, Inserm, CREATIS UMR 5220, U1206, F-69100, Villeurbanne, France

²Bioacoustics Research Laboratory, Department of Electrical and Computer Engineering, University of Illinois Urbana-Champaign, 306 N. Wright St., Urbana, IL 61801, USA.

Corresponding author:

Pauline Muleki-Seya, CREATIS, CNRS.

Email: pauline.muleki-seya@creatis.insa-lyon.fr

and mean relative errors $<5\%$ for the radius for 4T1, JC, LMTK and MAT *ex vivo* tumors. However, the mean relative errors were not very good for 4T1 and JC CP biophantoms.

Two additional models have been explored when both cells and their nuclei together were considered ultrasound scatterers. The concentric spheres model (CSM) [McNew et al. \(2009\)](#) yields incoherent scattering from an ensemble of concentric fluid spheres, taking into account the CSM's radii, densities, sound speeds, and number density. The CSM provided consistent results for low-concentration chinese hamster ovary (CHO) CP biophantoms [Teisseire et al. \(2010\)](#); [Han et al. \(2011\)](#), and further a better representation of 4T1 and MAT CP biophantoms and *ex vivo* tumors compared against a single fluid sphere model [Han et al. \(2013\)](#). The second combined cell-nucleus model [Muleki-Seya and O'Brien Jr. \(2022\)](#); [Muleki-Seya et al. \(2022\)](#) represented scattering from nuclei and cells as a linear contribution of the BSCs from nuclei and cells along with a nucleus-to-cell scattering ratio term. This model, denoted SFM2, took into account radius, volume fraction, relative impedance contrast from nucleus and cell scatterers separately, and a nucleus-to-cell scattering ratio.

For this study, the same optical histology and experimental ultrasound data acquired previously to gain a better understanding of the scattering sources [Muleki-Seya and O'Brien Jr. \(2022\)](#) were used. For estimating from histology nucleus and cell sizes, 2-D H&E-stained histology images were used. Because the microtome's blade does not generally intersect the nucleus and/or cell centers, only the largest measured nucleus and cell radii were used. While not ground truth, the approach used herein compares ultrasound-determined nucleus and cell radii to those of the histology-measured nucleus and cell radii.

Three ultrasound scattering models were compared using these previously acquired ultrasound and histology data from the 4T1, JC, LMTK and MAT CP biophantoms and *ex vivo* tumors. SFM [Muleki-Seya et al. \(2016\)](#) considers an ensemble of identical fluid spheres, SFM2 [Muleki-Seya and O'Brien Jr. \(2022\)](#) considers that in some cells, the main ultrasound scattering sites are the nuclei and for others, the cells themselves are the scattering sites, and CSM [McNew et al. \(2009\)](#) considers an ensemble of randomly positioned concentric-sphere scatterers, each concentric sphere consisting of an inner sphere and outer sphere to model a eukaryote cell. Thus, scatterer parameters from four cell lines of CP biophantoms and *ex vivo* tumors are estimated using SFM, SFM2 and CSM to evaluate quantitatively the degree to which these ultrasound scattering models provide scatterer values consistent with optical-measured histologic results. SFM and CSM have already been used to estimate scattering parameters on different cell lines and tissues for SFM [Muleki-Seya et al. \(2016\)](#); [Muleki-Seya and O'Brien Jr. \(2022\)](#) and on the CHO cell line for CSM [Teisseire et al. \(2010\)](#); [Han et al. \(2011\)](#). A first step of this study was presented in a conference paper [Muleki-Seya et al. \(2022\)](#), but herein, we specifically improve the constraints of the inverse approach to remove the nonphysical scatterer values (i.e., negative radius) and

provide a fairer comparison between SFM2 and CSM. Moreover, we study the inversion results of *ex vivo* tumors in addition to CP biophantoms. We also tested two different cost functions to which more or less weight to high ultrasound frequency weight is given.

Material and Methods

Ultrasound acquisitions

The CP biophantoms and tumors used in this study were the same as those used in [Muleki-Seya and O'Brien Jr. \(2022\)](#). They were composed of a large number of densely packed cells without any supportive background materials. Four tumor cell lines were used: 13762 MAT B III (MAT) mammary adenocarcinoma (ATCC CRL-1666), 4T1 mammary carcinoma (ATCC CRL-2539), JC mammary adenocarcinoma (ATCC CRL-2116) and LMTK soft-tissue sarcoma (ATCC CCL-1.3), denoted MAT, 4T1, JC and LMTK, respectively. 3 MAT, 16 4T1, 10 JC, and 15 LMTK independent CP biophantom replicates were present in this study. Tumors were grown in mice and rats (Harlan Laboratories, Inc., Indianapolis, IN) using the same CP cell lines: 13 Fischer 344 rats (MAT tumors), 20 BALB/c mice (13 mice with 4T1 tumors and 7 mice with JC tumors) and 8 Nude-Foxn1nu mice (LMTK tumors). After animal euthanasia, the tumors were excised and removed for *ex vivo* measurements. 18 MAT, 22 4T1, 10 JC, and 13 LMTK independent tumor replicates were present in this study. These CP biophantoms and tumors were used because previous results suggested ultrasound scattering from cells only from LMTK and MAT CP, from both cells and nuclei for 4T1 and JC CP, and from nuclei only from *ex vivo* tumors [Muleki-Seya and O'Brien Jr. \(2022\)](#).

The ultrasound scanning procedures were described in [Han et al. \(2013\)](#). Briefly, a single-element, weakly focused 40-MHz transducer (High-Frequency Transducer Resource Center, USC, Los Angeles, CA, -10 dB ultrasound bandwidth of 25–55 MHz) was used. For each CP biophantom sample, 11 independent ultrasound scans were recorded and a mean BSC was estimated for each of these 11 scans by averaging the BSCs from different regions-of-interest (ROIs) within that scan. Then, each mean BSC was used to estimate the scatterer parameters. Immediately after scanning, the sample was prepared for histology processing. Cell and nucleus radii and volume fractions were optically estimated from histology images of these CP biophantoms [Muleki-Seya and O'Brien Jr. \(2022\)](#).

Ultrasound scattering models

QUS estimates are compared from three models: SFM, SFM adapted for two scatterers (denoted SFM2) and CSM. These models were previously described in detail in [Muleki-Seya et al. \(2016\)](#) for SFM, in [Muleki-Seya and O'Brien Jr. \(2022\)](#) for SFM2 and in [McNew et al. \(2009\)](#); [Teisseire et al. \(2010\)](#) for CSM. These models are subject to several approximations: Born, far-field, incident plane wave, and isotropic medium. SFM and SFM2 consider the incoherent and coherent scattering fields, and the CSM considers only

the incoherent scattering field. For the three ultrasound models, monodisperse scatterer size is assumed.

SFM considers an ensemble of identical fluid spheres. This model is adapted for concentrated media by taking into account the Structure Factor term S that is related to scatterer spatial positions. SFM is based on the assumption that, at high scatterer volume fractions, interference effects are mainly caused by correlations between the spatial positions of individual scatterers. By considering an ensemble of identical spheres of radius a , the theoretical BSC for the SFM formulation is given by Twersky (1987); Franceschini and Guillermin (2012):

$$BSC_{SFM}(k) = n \frac{k^4 V_s^2 \gamma_Z^2}{4\pi^2} \left[\frac{3}{(2ka)^3} j_1(2ka) \right]^2 S(k); \quad (1)$$

where k is the wavenumber, V_s is the sphere volume and $n = \phi/V_s$ is the number density with ϕ the scatterer volume fraction, γ_Z is the relative impedance contrast between the scatterer and the surrounding medium and j_1 is the spherical Bessel function of the first kind of order 1. S is the Structure Factor, which is analytically obtained as described in Franceschini and Guillermin (2012); Wertheim (1963). The unknown parameters are the scatterer radius a , the volume fraction ϕ , and the relative impedance contrast γ_Z .

The second model considers the possibility that for some cells, the main ultrasound scattering sites are the nuclei, and for others, the cells themselves. For these conditions, the BSC from cells and nuclei BSC_{NC} using SFM2 is defined as Muleki-Seya and O'Brien Jr. (2022):

$$BSC_{NC}(k) = w BSC_N(k) + (1 - w) BSC_C(k) \quad (2)$$

where BSC_N and BSC_C are the BSCs from nuclei and cells only estimated with SFM (eq 1) and w is the nucleus-to-cell scattering ratio: $w = 0$ corresponds to scattering from cells only and $w = 1$ corresponds to scattering from nuclei only. The unknown parameters are the scatterer radii a_N and a_C , the volume fractions ϕ_N and ϕ_C , the relative impedance contrasts γ_{ZN} and γ_{ZC} and the nucleus-to-cell scattering ratio w . Because of the presence of the term w , the relative impedance contrasts estimated do not correspond to the relative impedance contrast estimated with SFM.

The CSM considers an ensemble of randomly positioned concentric-sphere scatterers (inner sphere denoted 2, outer sphere denoted 1 and background denoted 0). By assuming the coherent field is not taken into account and waves do not interfere, the BSC is written as Teisseire et al. (2010):

$$BSC_{CSM}(f) = nr^2 \frac{|p_{scatt}(\theta = \pi)|^2}{P_0^2} \quad (3)$$

where f is the frequency, r is the observation point, $p_{scatt}(\theta = \pi)$ is the backscattered ultrasound pressure and P_0 is the amplitude of the incident pressure. At an observation point r , the ultrasound pressure scattered from the two concentric spheres is given in McNew et al. (2009). The unknown parameters are the inner and outer scatterer radii a_2 and a_1 , the densities (ρ_0, ρ_1, ρ_2), the sound speeds (c_0, c_1, c_2), and the number density n . The outer and inner

volume fractions were evaluated from $\phi_1 = 4\pi a_1^3 n$ and $\phi_2 = 4\pi a_2^3 n$, respectively.

Scatterer parameter evaluations

Estimated values of the scatterer parameters were determined by fitting the measured BSC_{meas} to the theoretical BSCs, BSC_{theo} , by minimizing the cost function:

$$F = \frac{\sum_j \|BSC_{meas}(k_j) - BSC_{theo}(k_j)\|^2}{\sum_j BSC_{meas}(k_j)^2} \quad (4)$$

where BSC_{theo} is given by eq. 1, 2 or 3.

A second cost function giving less weight to errors at high ultrasound frequencies was also used, and is denoted the Log cost function:

$$F_{LOG} = \frac{\sum_j \|Log(BSC_{meas}(k_j)) - Log(BSC_{theo}(k_j))\|^2}{\sum_j Log(BSC_{meas}(k_j))^2} \quad (5)$$

This Log cost function was used for comparison only on CP biophantom data. The cost functions were minimized over 25–55 MHz. The fitting procedure was performed using the minimization routine *fminsearch*, which is without constraints and *fmincon*, which is with constraints (MATLAB, The MathWorks, Inc., Natick, MA). *fminsearch* is based on the Nelder-Mead simplex algorithm and *fmincon* on an interior-point algorithm. More specifically, *fminsearch* finds the minimum of a scalar function of several variables, starting at an initial estimate, and *fmincon* finds a constrained minimum of a scalar function of several variables starting at an initial estimate. Scatterer parameters using SFM with *fminsearch* optimization strategies were already presented in Muleki-Seya and O'Brien Jr. (2022). The best cost function was evaluated by testing 20 randomly defined initial conditions. The range of values for these initial conditions were $4 < a < 10 \mu\text{m}$, $0 < \phi < 0.7$, and $0.005 < \gamma_Z < 0.055$ for SFM; $1 < a_N < 7 \mu\text{m}$, $5 < a_C < 9 \mu\text{m}$, $0 < \phi_N < 0.3$, $0.45 < \phi_C < 0.75$, $0.005 < \gamma_{ZN,C} < 0.055$ and $0 < w < 1$ for SFM2; and $1 < a_2 < 7 \mu\text{m}$, $4 < a_1 < 9 \mu\text{m}$, $1 < \rho_{0,1,2} < 1.2 \text{ g/mL}$, $1500 < c_{0,1,2} < 1600 \text{ m/s}$, and $147 < n < 2700 \times 10^6$ scatterers/mL for CSM. The n range of values corresponds to scatterer volume fraction between 0.45 and 0.75 for a_1 radii.

For *fminsearch*, initial conditions yielding negative radii, volume fraction, or relative impedance contrast as well as volume fraction greater than 1 were not used. For *fmincon* optimization strategy, the constraints used were adapted for nuclei and/or cells. The constraint ranges were defined as large as possible with limited overlap between nuclear and cell radii and volume fractions. The maximum relative impedance contrast constraints were defined as 0.2, which seems reasonable given the results in the literature Franceschini et al. (2014); Yuan and Shung (1988). The densities and sound speed constraints correspond to tissue values. These constraints were $3 < a < 10 \mu\text{m}$, $0.05 < \phi < 0.8$, and $0 < \gamma_Z < 0.2$ for SFM. The constraints used for SFM2 were $3 < a_N < 6.5 \mu\text{m}$, $5.5 < a_C < 10 \mu\text{m}$, $0.05 < \phi_N < 0.3$, $0.4 < \phi_C < 0.8$, $0 < \gamma_{ZN,C} < 0.5$

and $0 < w < 1$. The constraints used for CSM were $3 < a_2 < 6.5 \mu\text{m}$, $5.5 < a_1 < 10 \mu\text{m}$, $0.9 < \rho_{0,1,2} < 1.2 \text{ g/mL}$, $1450 < c_{0,1,2} < 1630 \text{ m/s}$, and $40 < n < 2700 \times 10^6$ scatterers/mL. For CSM, initial conditions yielding $0.05 > \phi_1 > 0.3$, $0.4 > \phi_2 > 0.8$, $0 > |\rho_1 c_1 - \rho_0 c_0| / \rho_0 c_0 > 0.2$ or $0 > |\rho_2 c_2 - \rho_1 c_1| / \rho_1 c_1 > 0.2$ were not used. The goodness-of-fit statistic R^2 was calculated Oelze and O'Brien Jr. (2006). R^2 (range between 0 and 1) describes how well a model fits the experimental data for which 1 denotes the best experimental model data fit. In the following, we are interested in the a and ϕ parameters and their distributions. The ρ and c values have been chosen to be in the biological tissue range.

Results

H&E-based backscatter coefficients for SFM, SFM2 and CSM

Cell and nucleus radii and their respective volume fractions from 4T1, JC, LMTK and MAT CP biophantom and *ex vivo* tumors histologic results were presented in Table III from Muleki-Seya and O'Brien Jr. (2022). These radii and volume fractions were evaluated from 2D optical-measured histology images.

H&E-based BSCs for SFM, SFM2 and CSM using their mean nucleus and cell radii and their respective volume fractions are presented in Figure 1 as well as the measured BSCs for each cell line CPs and tumors. To obtain these calculated BSCs, an *fminsearch* optimization strategy was used for the impedance contrast parameter or densities and sound speeds for CSM. Note that the relative impedance contrast affects the amplitude of the BSC. These models provided calculated BSCs included within the range of measured BSCs, except for the SFM for scattering from cells for 4T1 and JC CP biophantoms. For tumors, calculated BSCs are included within the range of measured BSCs except for the SFM for scattering from cells for the four cell lines.

(a, ϕ) scatterer parameter distributions obtained with SFM, SFM2 and CSM

An example of the (a, ϕ) scatterer parameter distributions obtained for 4T1 CP biophantoms using SFM, SFM2 and CSM is presented in Figure 2 using *fminsearch* and *fmincon* optimization strategies. (a, ϕ) scatterer parameter distributions obtained for all cell lines using *fminsearch* and *fmincon* optimization strategies are presented in Figures A1 and A2 in Appendix. For both optimization strategies, the (a, ϕ) distributions estimated with SFM are quite variable and are not well centered around the nucleus or cell values except for MAT CP biophantoms where the (a, ϕ) distribution is centered around the cell radius and volume fraction values estimated from histology. The models adapted for cell and nucleus scatterer parameter estimations, SFM2 and CSM, allow for the evaluation of two (a, ϕ) distributions with mean values centered around the mean nucleus and cell radii and volume fractions estimated from histology. The goodness-of-fit obtained with SFM, SFM2 and CSM were similar for the three models (R^2

mean > 0.98 for SFM, > 0.95 for SFM2 and > 0.98 for CSM).

(a, ϕ) scatterer parameter distributions obtained for 4T1, JC, LMTK and MAT CP biophantoms using *fminsearch* and *fmincon* optimization strategies with the Log cost function are presented in Figures A3 and A4 in Appendix. SFM and SFM2 provided (a, ϕ) distributions which are quite variable and are not well centered around the nucleus or cell values except for MAT CP biophantoms where the (a, ϕ) distribution is centered around the cell radius and volume fraction values estimated from histology. CSM allow for the evaluation of two (a, ϕ) distributions with mean values centered around the mean nucleus and cell radii and volume fractions estimated from histology. The goodness-of-fit obtained with SFM, SFM2 and CSM were similar for the three models (R^2 mean > 0.96 for SFM, > 0.93 (except for MAT with *fminsearch* optimization strategy R^2 mean = 0.82) for SFM2 and > 0.93 for CSM).

An example of the (a, ϕ) scatterer parameter distributions obtained for 4T1 Tumors using SFM, SFM2 and CSM is presented in Figure 3 using *fminsearch* and *fmincon* optimization strategies. (a, ϕ) scatterer parameter distributions obtained for all cell lines using *fminsearch* and *fmincon* optimization strategies are presented in Figures A5 and A6 in Appendix. These distributions behave similarly to those of biophantoms. CSM provided mean values more centered around the mean nucleus and cell radii and volume fractions estimated from histology than SFM2. The goodness-of-fit obtained with SFM, SFM2 and CSM were similar for the three models (R^2 mean > 0.85 for SFM, > 0.79 for SFM2 and > 0.89 for CSM).

Mean radius and volume fraction parameters

Mean radius and volume fraction scatterer parameter values were evaluated with SFM (a single distribution), SFM2 and CSM (nucleus and cell distributions) for the four cell lines and both optimization strategies. For each parameter distribution, the nucleus or cell radius and volume fraction relative error was evaluated where the relative error is the ratio of the absolute error of a parameter estimate from histology ($|\langle QUS \rangle - \langle histo \rangle|$) to the histology of this parameter estimate ($\langle histo \rangle$), where $\langle QUS \rangle$ denotes the mean QUS-derived scattering parameter (radius and volume fraction) and $\langle histo \rangle$ denotes the mean histology-derived parameter. The relative error ranges between 0% and 100% for which 0% denotes perfect correspondence of the ultrasound estimates to the histology-derived parameter (Table III from Muleki-Seya and O'Brien Jr. (2022)). These relative error results are summarized in Table 1. In all cases, the models adapted for two scatterers provided mean parameters closer to histology values when the nucleus and cell radii and volume fraction were processed together. However, when these parameters were considered individually (scatterer nucleus radius or scatterer nucleus volume fraction, or scatterer cell radius or scatterer cell volume fraction), SFM may provide a lower relative error (value closer to 0%) than SFM2 and CSM as for JC nucleus radius estimates for example. Using constraints (*fmincon*) makes it possible to reduce these

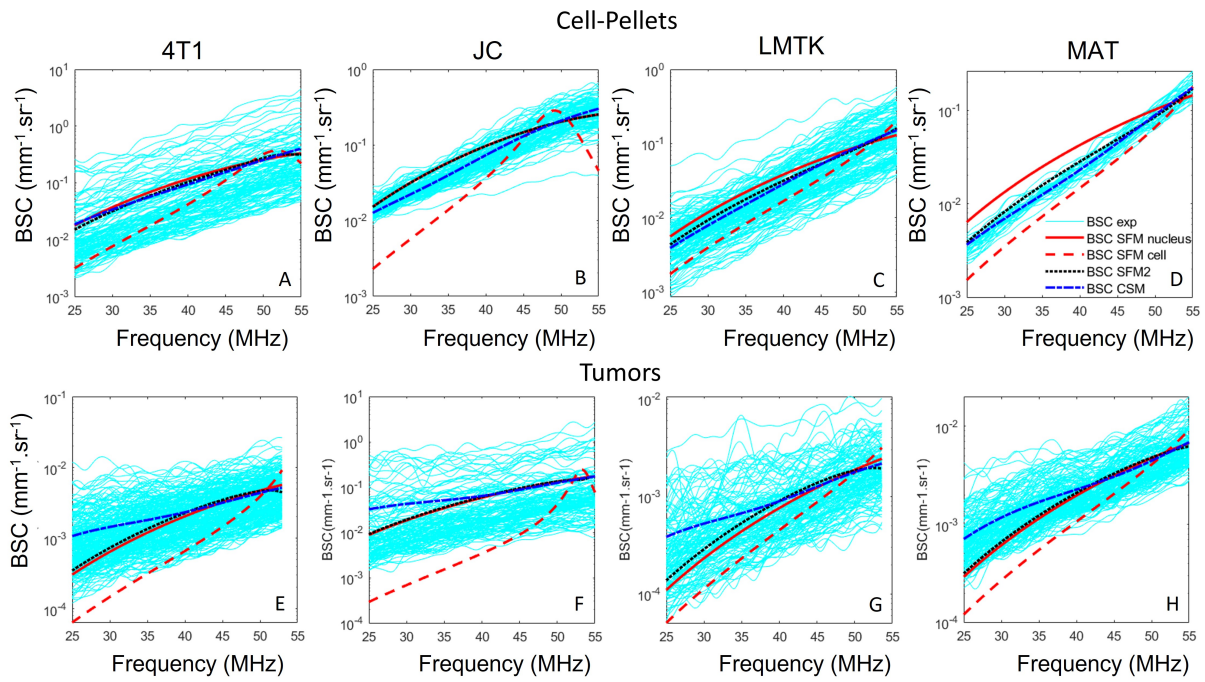


Figure 1. Experimental and H&E-based BSCs for 4T1, JC, LMTK and MAT CP biophantoms (A-D) and tumors (E-H). For the H&E-based BSCs presented for SFM, SFM2 and CSM, the nucleus/cell ratio and volume fractions were the mean parameters from optical-measured histology.

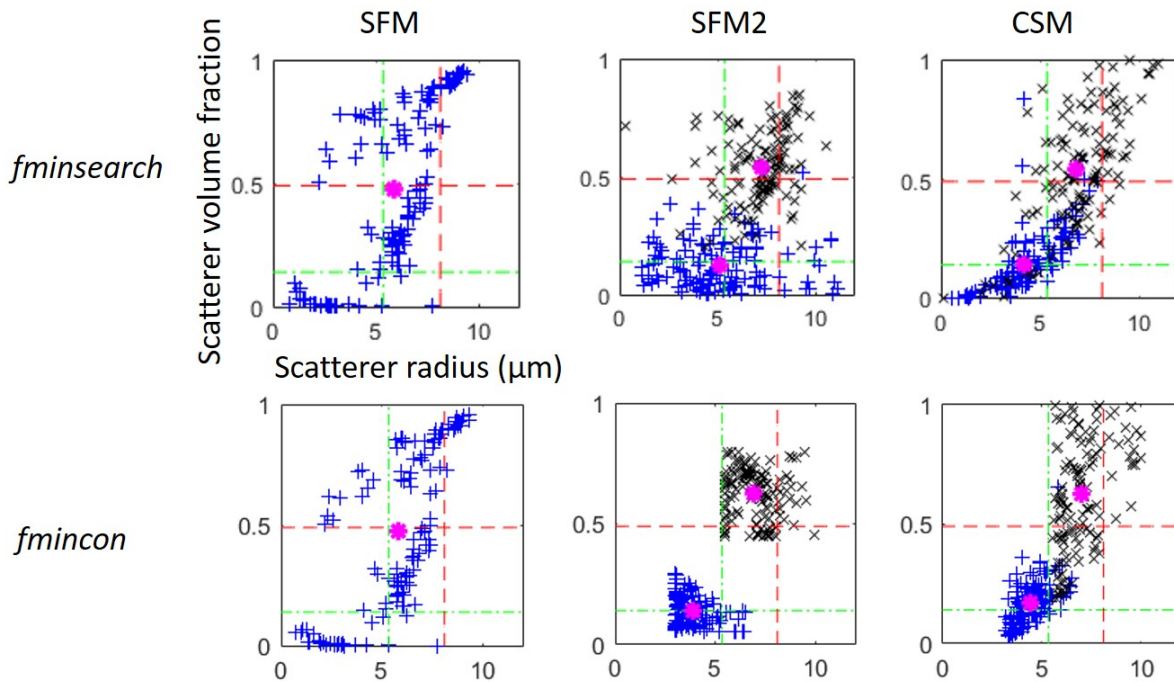


Figure 2. Scatterer radius vs. volume fraction for 4T1 CP biophantoms obtained with SFM (first column), SFM2 (second column) and CSM (third column) with *fminsearch* (first row) and *fmincon* (second row) optimization strategies. For SFM2 and CSM, blue +: scatterers correspond to nuclei, and black x: scatterers correspond to cells. The magenta asterisks correspond to the mean value of each distribution. The green (a_N & ϕ_N) and red (a_C & ϕ_C) dashed lines correspond to the mean optical-measured histology nucleus and cell radii and volume fractions from [Muleki-Seya and O'Brien Jr. \(2022\)](#), respectively.

average relative errors but to the detriment of one or more parameters generally (Table 1).

The mean radius and volume fraction relative error results using the Log cost functions for CP biophantoms are summarized in Table A1 in Appendix. Globally, relative

error values with this Log cost function are of the same order of magnitude using SFM, much higher with SFM2 and a little higher with CSM. For CSM and SFM2, the average values obtained with this cost function then provided a poorer match to the value obtained from the histology than

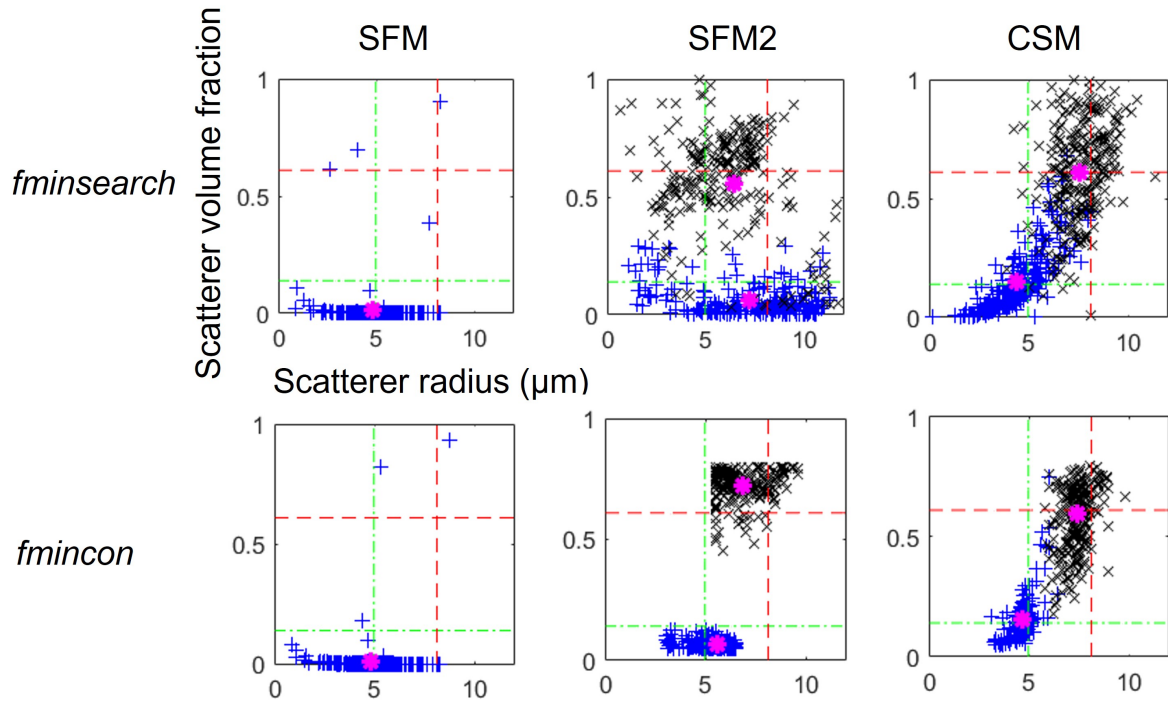


Figure 3. Scatterer radius vs. volume fraction for 4T1 tumors obtained with SFM (first column), SFM2 (second column) and CSM (third column) with *fminsearch* (first row) and *fmincon* (second row) optimization strategies. For SFM2 and CSM, blue +: scatterers correspond to nuclei, and black x: scatterers correspond to cells. The magenta asterisks correspond to the mean value of each distribution. The green (a_N & ϕ_N) and red (a_C & ϕ_C) dashed lines correspond to the mean optical-measured histology nucleus and cell radii and volume fractions from [Muleki-Seya and O'Brien Jr. \(2022\)](#), respectively.

Relative error (%)	SFM				SFM2				CSM			
	Nucleus		Cell		Nucleus		Cell		Nucleus		Cell	
	a	ϕ	a	ϕ	a	ϕ	a	ϕ	a	ϕ	a	ϕ
<i>fminsearch</i>												
4T1	9	239	28	3	4	10	11	9	23	3	11	15
JC	6	153	33	37	20	15	13	15	7	51	9	22
LMTK	43	235	8	13	17	4	<1	11	3	27	3	2
MAT	62	274	6	16	12	32	<1	12	5	31	17	16
<i>fmincon</i>												
4T1	7	176	39	21	26	8	15	35	19	2	11	29
JC	7	129	41	43	29	27	28	27	10	20	9	24
LMTK	12	164	28	32	18	16	8	15	3	2	3	10
MAT	50	288	13	13	8	54	3	7	0	22	10	3

Table 1. Relative errors of the mean nucleus and cell radius and volume fraction estimates from CP biophantoms using optical-measured histology as the approximated ground truth for SFM, SFM2 and CSM and with both *fminsearch* (without constraints) and *fmincon* (with constraints) optimization strategies. Results in bold highlight relative errors less than 20%

did the linear cost function.

The mean radius and volume fraction relative error results for tumors are summarized in Table 2. The SFM estimates of scatterer radius are very close to nucleus radius. CSM provided a better match to the value obtained from the histology than SFM2.

Coefficient of variation estimates

The variability of the scatterer parameter distribution was estimated using the coefficient of variation (ratio of the standard deviation of the replicates of a cell line to the mean for that cell line), also known as the normalized root-mean-square deviation, which is a measurement of the

dispersion of a distribution. A lower coefficient of variation (less disperse) suggests a better model fit. The coefficient of variation obtained for radius and volume fraction estimates of 4T1, JC, LMTK and MAT CP biophantoms with SFM, SFM2 and CSM are presented in Table 3. Using *fminsearch* optimization strategy, scattering models adapted for two scatterers (SFM2 and CSM) do not reduce the coefficients of variation of the estimates. For SFM2 and CSM, the coefficient of variation for the cell distributions is lower than that from SFM, but the coefficient of variation for the nucleus distributions is higher. Using constraints, with *fmincon*, tend to reduce the coefficient of variation for each model but mostly for SFM2 and CSM, which provided lower coefficients of variation than SFM. This is probably because

Relative error (%)	SFM				SFM2				CSM			
	Nucleus		Cell		Nucleus		Cell		Nucleus		Cell	
	a	ϕ	a	ϕ	a	ϕ	a	ϕ	a	ϕ	a	ϕ
<i>fminsearch</i>												
4T1	37	247	16	20	25	22	11	16	12	7	7	<1
JC	5	35	44	85	15	27	23	12	8	37	12	2
LMTK	5	53	39	88	28	54	16	6	8	11	6	3
MAT	1	37	40	86	62	57	8	13	11	4	3	5
<i>fmincon</i>												
4T1	4	50	36	89	12	55	16	19	5	11	8	2
JC	2	12	41	79	1	39	20	17	9	11	12	12
LMTK	3	23	35	81	9	53	6	12	4	4	2	7
MAT	4	10	37	80	17	50	3	14	5	17	1	<1

Table 2. Relative errors of the mean nucleus and cell radius and volume fraction estimates from tumors using optical-measured histology as the approximated ground truth for SFM, SFM2 and CSM and with both *fminsearch* (without constraints) and *fmincon* (with constraints) optimization strategies. Results in bold highlight relative errors less than 20%

the ranges of these estimates are drastically reduced based on the constraints defined. Indeed, the range of scatterer parameter values with SFM2 and CSM is lower than with SFM ($3 < a < 10 \mu\text{m}$ for SFM and $3 < a_N < 6.5 \mu\text{m}$ and $5.5 < a_C < 10 \mu\text{m}$ for SFM2 and CSM for the scatterer radii for example).

The coefficient of variation obtained for radius and volume fraction estimates of CP biophantoms using the Log cost functions are summarized in Table A2 in Appendix. Globally, coefficient of variation with the Log cost function are higher than with the linear cost function.

The coefficient of variation obtained for radius and volume fraction estimates of tumors are summarized in Table 4. As for the CP biophantoms, scattering models adapted for two scatterers (SFM2 and CSM) do not reduce the coefficients of variation of the estimates and using *fmincon* tends to reduce the coefficient of variation for each model.

Percentage of "correct" nucleus and cell estimates

The definition for a "correct" nucleus (cell) estimate corresponds to an estimation of the scatterer radius and volume fraction both with less than 20% of relative error with the nucleus (cell) radius and volume fraction from optical-measured histology (see black rectangles areas in Figure 4). The 20% criterion was chosen based on the maximum relative error estimated of cell and nucleus radii from histology (Table III of Muleki-Seya and O'Brien Jr. (2022)) which were from 8 to 21%.

The percentage of "correct" nucleus and cell estimates with SFM, SFM2 and CSM with and without constraints in the optimization approach is summarized in Table 5. SFM2 and CSM yield a higher percentage of correct cell parameters. For example, for LMTK CP biophantoms with *fminsearch*, 2.42% of correct cell parameters were estimated with SFM, 35.8% with SFM2 and 33.3% with CSM. Without constraints (*fminsearch*), percentages of correct cell parameters are lower with CSM than with SFM2 but percentages of correct nuclei are higher. With constraints (*fmincon*), percentages of correct nucleus and

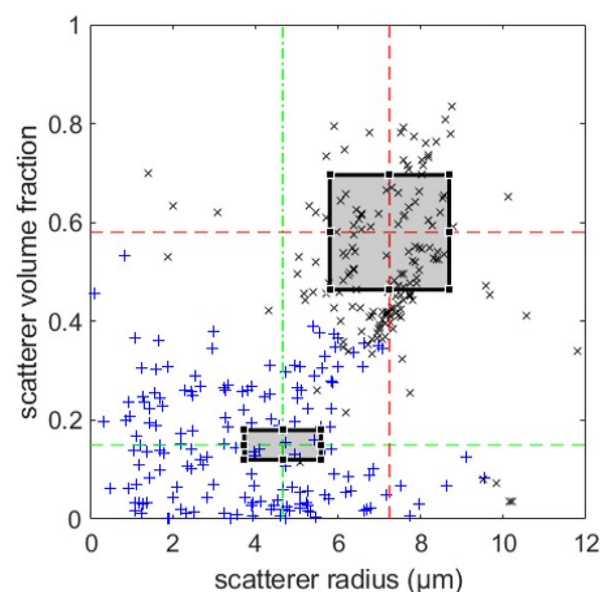


Figure 4. Example of (a, ϕ) distributions with black rectangles corresponding to the area of the correct nucleus and cell estimates for LMTK CP and SFM2 model with *fminsearch* strategy. Correct estimates are defined as the mean radius and volume fraction ± 0.2 times the mean radius and volume fraction. The green (a_N & ϕ_N) and red (a_C & ϕ_C) dashed lines correspond to the mean optical-measured histology nucleus and cell radii and volume fractions from Muleki-Seya and O'Brien Jr. (2022), respectively.

cell parameters are higher with CSM than with SFM2. When using constraints, the percentage of correct estimates with SFM is not better than without constraints. The percentage of correct nucleus parameters estimated with SFM2 increased and the percentage of correct cell parameters increased also for LMTK and MAT CP biophantoms but decrease for 4T1 and JC. Using constraints, the percentage of correct nucleus estimates increased with CSM and the percentage of correct cell estimates increased also except for JC CP biophantoms. CSM yielded a higher percentage of simultaneously correct nuclei and cells than SFM2 for both optimization strategies but mostly with *fmincon* (4.85% of correct nuclei and cells estimates where found for LMTK using SFM2 with *fmincon*

Coefficient of variation	SFM		SFM2				CSM				
			Nucleus		Cell		Nucleus		Cell		
	a	ϕ	a	ϕ	a	ϕ	a	ϕ	a	ϕ	
<i>fminsearch</i>											
4T1	0.36	0.69	0.49	0.78	0.23	0.28	0.41	1.09	0.23	0.38	
JC	0.27	0.58	0.52	0.65	0.21	0.28	0.33	0.83	0.17	0.36	
LMTK	0.25	0.57	0.52	0.76	0.24	0.32	0.38	0.84	0.20	0.35	
MAT	0.08	0.26	0.58	0.80	0.18	0.23	0.31	1.03	0.13	0.36	
<i>fmincon</i>											
4T1	0.26	0.56	0.20	0.36	0.13	0.12	0.16	0.32	0.14	0.18	
JC	0.25	0.52	0.19	0.33	0.14	0.13	0.18	0.32	0.15	0.18	
LMTK	0.19	0.42	0.16	0.32	0.11	0.11	0.15	0.29	0.13	0.17	
MAT	0.10	0.22	0.19	0.29	0.07	0.13	0.08	0.25	0.07	0.19	

Table 3. Coefficients of variation obtained for radius and volume fraction estimates of 4T1, JC, LMTK and MAT CP biophantoms using SFM, SFM2 and CSM for *fminsearch* and *fmincon* optimization strategies. For SFM2 and CSM, the two coefficients of variation for the radius and the volume fraction correspond to those related to the nucleus and cell estimates.

Coefficient of variation	SFM		SFM2				CSM			
			Nucleus		Cell		Nucleus		Cell	
	a	ϕ	a	ϕ	a	ϕ	a	ϕ	a	ϕ
<i>fminsearch</i>										
4T1	0.08	0.26	0.58	0.80	0.18	0.23	0.32	0.88	0.15	0.36
JC	0.35	1.94	0.42	0.96	0.39	0.43	0.38	0.99	0.23	0.39
LMTK	0.39	2.84	0.50	1.13	0.47	0.35	0.40	0.89	0.19	0.36
MAT	0.36	2.83	0.36	1.06	0.35	0.36	0.34	1.02	0.21	0.40
<i>fmincon</i>										
4T1	0.23	1.46	0.18	0.27	0.14	0.08	0.09	0.51	0.09	0.54
JC	0.25	1.18	0.21	0.42	0.17	0.12	0.16	0.53	0.13	0.62
LMTK	0.27	1.57	0.24	0.37	0.15	0.11	0.10	0.64	0.11	0.83
MAT	0.24	1.57	0.24	0.40	0.16	0.11	0.12	0.45	0.11	0.74

Table 4. Coefficients of variation obtained for radius and volume fraction estimates of 4T1, JC, LMTK and MAT tumors using SFM, SFM2 and CSM for *fminsearch* and *fmincon* optimization strategies. For SFM2 and CSM, the two coefficients of variation for the radius and the volume fraction correspond to those related to the nucleus and cell estimates.

and 29.6% using CSM).

The percentage of "correct" nucleus and cell estimates of CP biophantoms using the Log cost functions are summarized in Table A3 in Appendix. Except for LMTK and MAT cell estimates using SFM2 and *fminsearch* optimization strategy, the percentages of correct estimates are generally lower when using the Log cost function.

The percentage of "correct" nucleus and cell estimates of tumors are summarized in Table 6. As for the CP biophantoms, SFM2 and CSM yield a higher percentage of correct parameters than SFM but mostly CSM. Using *fmincon* allow to increase the percentage of correct cell parameters with SFM2 but to increase both percentages of correct cell and nuclei parameters with CSM.

Discussion

The objective of this study was to determine whether ultrasound scattering models adapted for combined nucleus and cell scatterers provided identification and better quantification of scatterer parameters than SFM. Three criteria were evaluated: 1) relative error between the mean values of nucleus and cell radii and volume fractions estimates with histology-derived values, 2) coefficient of

variation of each estimate, and 3) percentage of correct nuclei and cell estimates. This study is based on previously published data from cell-pellet (CP) biophantoms and *ex vivo* tumors from four cell lines [Muleki-Seya and O'Brien Jr. \(2022\)](#).

The two evaluated models (SFM2 and CSM) contained 7 and 9 variables, respectively. For comparison, volume fraction was quantified from CSM models and only the nucleus and cell radii and volume fractions were compared to the nucleus and cell radii and volume fractions estimated from histology. For SFM, the scatterer radius and volume fraction were also compared to nucleus and cell radii and volume fractions estimated from histology. SFM and SFM2 take into account the incoherent and coherent scattering from a single monodisperse or two monodisperse scatterer distributions and are adapted for concentrated media. CSM considered only the incoherent scattering from an ensemble of concentric fluid spheres and may be better adapted for diluted media. Han et al [Han et al. \(2011\)](#), observed that the estimated parameter and mostly the inner and outer radii were not as well estimated for cell concentrations (volume densities, mL/mL) of 30% and 63% compared to cell concentrations lower than 10% for CHO CP biophantoms.

Correct (%)	SFM		SFM2			CSM		
	N	C	N	C	NC	N	C	NC
<i>fminsearch</i>								
4T1	4	8	2	39	2	10	17	2
JC	1	0	2	36	1	4	17	1
LMTK	1	2	5	36	2	10	22	3
MAT	0	9	0	48	0	15	27	6
<i>fmincon</i>								
4T1	3	6	9	12	1	14	26	9
JC	1	0	5	14	0	15	17	8
LMTK	2	7	16	46	5	45	52	30
MAT	0	45	3	82	3	30	61	21

Table 5. Percentage of "correct" nucleus (N) and cell (C) and simultaneous nucleus and cell (NC) estimates using SFM, SFM2 and CSM for 4T1, JC, LMTK and MAT CP biophantoms with both *fminsearch* and *fmincon* optimization strategies. Results in bold highlight designate when a higher percentage of correct estimates was obtained using *fmincon* instead of *fminsearch*.

Correct (%)	SFM		SFM2			CSM		
	N	C	N	C	NC	N	C	NC
<i>fminsearch</i>								
4T1	0	0	1	17	0	14	39	6
JC	3	0	5	20	0	10	38	5
LMTK	0	0	0	24	0	14	39	7
MAT	0	1	3	31	0	9	31	6
<i>fmincon</i>								
4T1	0	0	2	51	1	49	60	35
JC	5	0	6	32	1	42	57	29
LMTK	1	0	3	61	1	37	49	26
MAT	0	1	2	61	2	31	57	15

Table 6. Percentage of "correct" nucleus (N) and cell (C) and simultaneous nucleus and cell (NC) estimates using SFM, SFM2 and CSM for 4T1, JC, LMTK and MAT tumors with both *fminsearch* and *fmincon* optimization strategies. Results in bold highlight designate when a higher percentage of correct estimates was obtained using *fmincon* instead of *fminsearch*.

Cell-pellet biophantoms are only composed of cells (without any supportive material) and the studied tumors are mostly of cells within the extracellular matrix, so the principal scattering sources should be nuclei and/or cells. By using mean radii and volume fractions from histology, SFM, SFM2 and CSM yield calculated BSCs in the range of measured BSCs for the four cell types except for SFM for scattering from cells for 4T1 and JC CP biophantoms and for the four tumors models. From BSC measurements, scatterer parameters quantified from SFM (a, ϕ) did not correlate particularly well with cells or nuclei except for MAT (Figures 2 for 4T1 distributions). SFM2 provided distributions centered around the mean nucleus and cell radii and volume fractions estimated from histology either with *fminsearch* or *fmincon* optimization strategies for the studied CP biophantoms and CSM provided distributions centered around the mean nucleus and cell radii and volume fractions estimated from histology for the studied CP biophantoms and tumors. SFM2 and CSM, even without constraints, improved the relative errors on each set of radius/volume fraction parameters for nuclei and cells compared to SFM (Table 1 and 2). Using *fmincon* yielded mixed relative error results. CSM provided lower relative errors than SFM2 for the studied tumors. In a previous study Muleki-Seya and O'Brien Jr. (2022), we concluded that 4T1, JC, LMTK and MAT correspond to dilute media with scattering mainly from the nucleus. In the case of dilute media, volume fraction estimation with SFM and SFM2 is likely to be incorrect Muleki-Seya et al. (2016). However, a dilute media condition will favor a better parameter estimation for CSM

according to Han et al. Han et al. (2011). This may explain why CSM provided better results than SFM2 for tumors (which is not the case for CP biophantoms). Concerning the CP biophantoms, no clear differences between 4T1 and JC in one hand and LMTK and MAT in another hand were observed which may reflect the difference in main scattering source (nuclei and cells for 4T1 and JC and cells for LMTK and MAT) suggested in Muleki-Seya and O'Brien Jr. (2022).

SFM2 and CSM did not improve the coefficients of variation of the estimates compared to SFM with *fminsearch* (Table 3 and 4). If constraints are added to the optimization strategy, these coefficients of variation are improved. Better results were obtained with CSM and SFM2 than with SFM, likely because for SFM, the constraints were defined to satisfy nucleus and cell scatterers and for SFM2 and CSM they were chosen to satisfy nucleus or cell scatterers.

In this study, we define a correct "less than 20% of error" criterion for which SFM2 and CSM models yield the higher rates of correct parameters (Table 5 and 6). Adding constraints in the optimization strategy increased the percentages of correct estimates, especially for the nuclei, but also for the cells for CSM and in some cases for SFM2 for CP biophantoms. The percentage of correct nuclei remained lower than those for cells, likely due to the size of the correct detection region which was based on a fraction of the values larger for cells (see Figure 4). For tumors, adding constraints increased the percentages of correct cell

estimates and also nuclei estimates for CSM.

For CP biophantoms, two cost functions were studied: a linear one already used in [Muleki-Seya et al. \(2016\)](#); [Muleki-Seya and O'Brien Jr. \(2022\)](#); [Muleki-Seya et al. \(2022\)](#) and a logarithmic one [Gerig et al. \(2004\)](#). The linear one gives more weight to high frequencies. Globally, the results with the Log cost function on CP biophantoms are less good: the relative errors are rather higher, and the percentages of correct estimates were rather lower.

The ultrasound scattering models proposed in this study are complex and depend on a large number of parameters. For this reason, we evaluate them with simple biological samples (CP biophantoms and *ex vivo* tumors mostly composed of cells within the extracellular matrix) whose scattering structures were targeted principally to be the nucleus and/or the cell. The next step will be to evaluate whether these models can yield good results in more complex tissues such as more complex tumors or *in vivo* vascularized tumors. Depending on the type of tumor, the tissue may consist almost entirely of tumor cells, or of tumor cells with the presence of, for example, acini or lobules and blood vessels. In the latter case, ground truth is more complicated. These models represent scattering from the nucleus and the cell, and the ultrasound acquisitions must be high enough frequency to provide scattering at the cellular scale. These frequencies are not used in clinical practice due to the very low tissue penetration obtained at such high frequencies (for example, for a ka value between 0.5 and 1.2, frequencies up to 24 MHz are required for scattering from cells with a radius of 5 μm). However, acquisitions at high frequencies (>15 MHz) can be realized for dermatology applications or possibly for organ imaging during a surgical procedure.

presented in Figures [A1](#) for *fminsearch* and [A2](#) for *fmincon* optimization strategies.

Conclusion

These overall results highlight the capability of QUS to identify scattering sites and additionally to quantify the accuracy and size of the scattering sites. Herein, it has been determined that SFM2 and CSM yield lower relative errors for nucleus and cell radii and volume fractions than SFM for 4T1, JC, LMTK and MAT CP biophantoms. For tumors, CSM provided lower relative errors than SFM2. In conclusion, the percentage of correct nucleus and cell size estimates are generally better with SFM2 and CSM than SFM for 4T1, JC, LMTK and MAT CP biophantoms and tumors. CSM provided higher percentages of correct estimates than SFM2 for tumors. The next step of this study will be to evaluate these models with more clinically relevant tissues such as tumors.

Acknowledgments

Appendix

QUS-derived scatterer parameter distributions from CP

The (a, ϕ) scatterer parameter distributions obtained for the CP biophantoms using SFM, SFM2 and CSM are

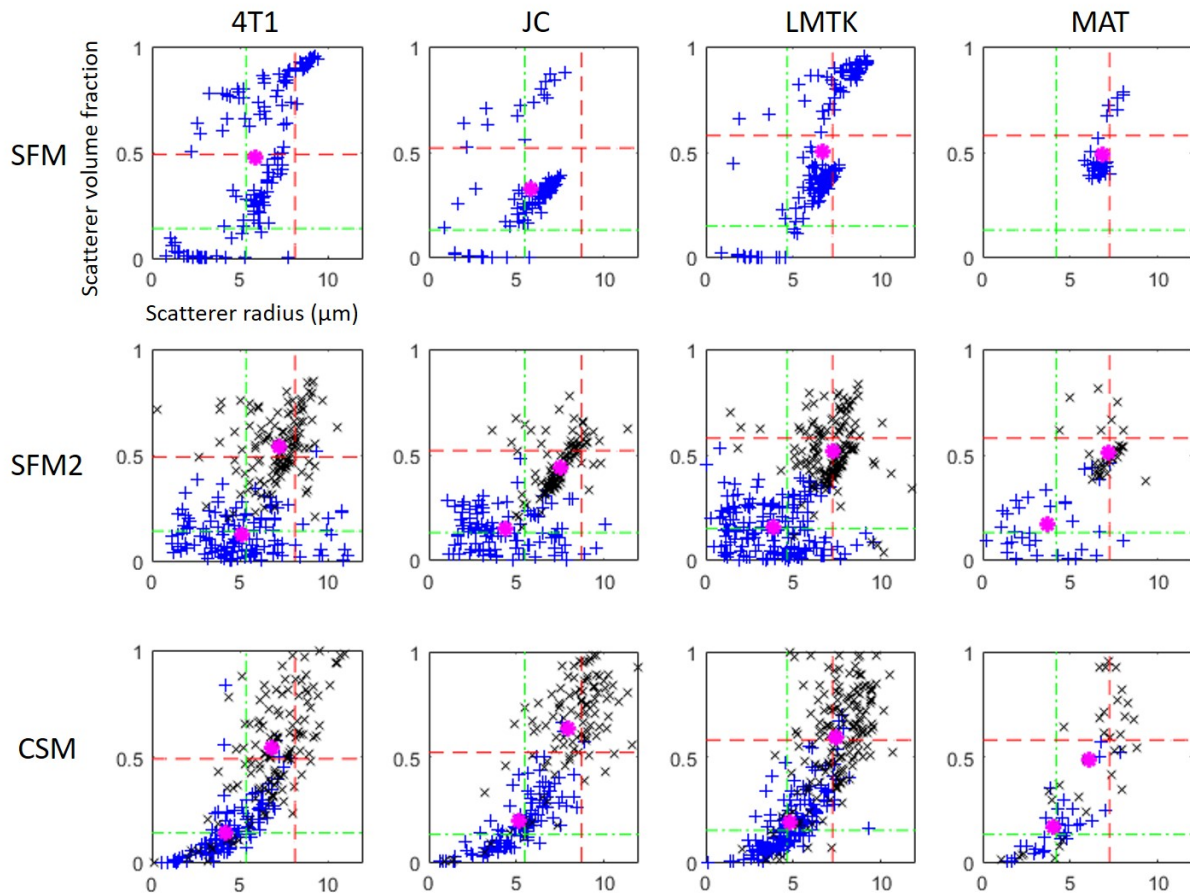


Figure A1. Scatterer radius vs. volume fraction for 4T1 (first row), JC (second row), LMTK (third row) and MAT (fourth row) CP biophantoms obtained with SFM (first line), SFM2 (second line) and CSM (third line) with *fminsearch* optimization strategy. For SFM2 and CSM, blue +: scatterers correspond to nuclei, and black x: scatterers correspond to cells. The magenta asterisks correspond to the mean value of each distribution. The green (a_N & ϕ_N) and red (a_C & ϕ_C) dashed lines correspond to the mean optical-measured histology nucleus and cell radii and volume fractions from Muleki-Seya and O'Brien Jr. (2022), respectively.

QUS-derived scatterer parameter distributions from CP with the log cost function

The (a, ϕ) scatterer parameter distributions obtained for the CP biophantoms using SFM, SFM2 and CSM with the Log cost function are presented in Figures A3 for *fminsearch* and A4 for *fmincon* optimization strategies.

The mean radius and volume fraction relative errors are summarized in Table A1.

The coefficient of variation obtained for radius and volume fraction estimates of 4T1, JC, LMTK and MAT CP biophantoms with SFM, SFM2 and CSM for the Log cost function are presented in Table A2.

The percentage of "correct" nucleus and cell estimates with SFM, SFM2 and CSM with and without constraints in the optimization approach for the Log cost function is summarized in Table A3.

QUS-derived scatterer parameter distributions from tumors

The (a, ϕ) scatterer parameter distributions obtained for the tumors using SFM, SFM2 and CSM are presented in

Figures A5 for *fminsearch* and A6 for *fmincon* optimization strategies.

References

- Franceschini E and Guillermin R (2012) Experimental assessment of four ultrasound scattering models for characterizing concentrated tissue-mimicking phantoms. *The Journal of the Acoustical Society of America* 132(6): 3735–3747.
- Franceschini E, Guillermin R, Tourniaire F, Roffino S, Lamy E and Landrier JF (2014) Structure factor model for understanding the measured backscatter coefficients from concentrated cell pellet biophantoms. *The Journal of the Acoustical Society of America* 135(6): 3620–3631.
- Gerig A, Varghese T and Zagzebski J (2004) Improved parametric imaging of scatterer size estimates using angular compounding. *IEEE Transactions on Ultrasonics, Ferroelectrics, and Frequency Control* 51(6): 708–715. DOI:10.1109/TUFFC.2004.1304269. URL <https://ieeexplore.ieee.org/abstract/document/1320851>. Conference Name: IEEE Transactions on Ultrasonics, Ferroelectrics, and Frequency Control.
- Han A, Abuhabsah R, Blue JP, Sarwate S and O'Brien Jr WD (2011) Ultrasonic backscatter coefficient quantitative estimates from high-concentration Chinese hamster ovary cell pellet

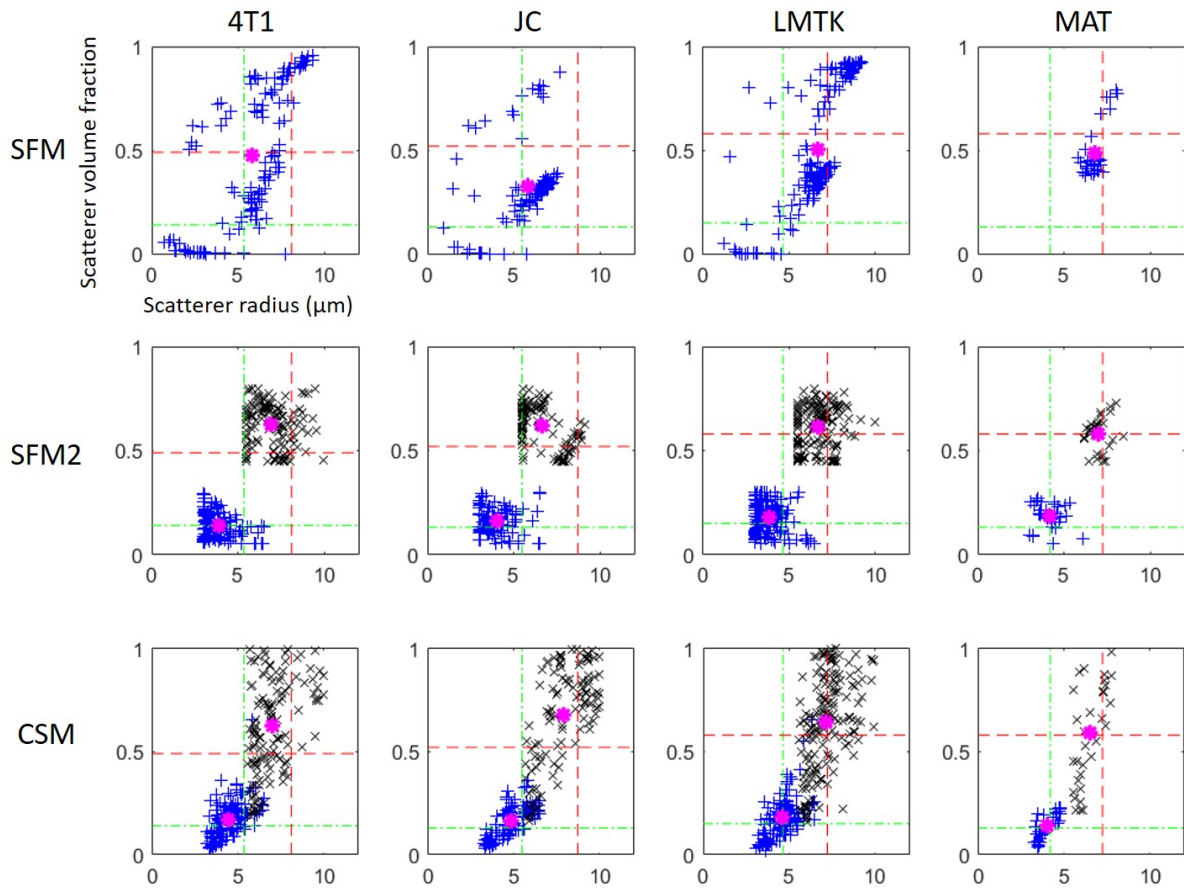


Figure A2. Scatterer radius vs. volume fraction for 4T1 (first row), JC (second row), LMTK (third row) and MAT (fourth row) CP biophantoms obtained with SFM (first line), SFM2 (second line) and CSM (third line) with *fmincon* optimization strategy. For SFM2 and CSM, blue +: scatterers correspond to nuclei, and black x: scatterers correspond to cells. The magenta asterisks correspond to the mean value of each distribution. The green (a_N & ϕ_N) and red (a_C & ϕ_C) dashed lines correspond to the mean optical-measured histology nucleus and cell radii and volume fractions from Muleki-Seya and O'Brien Jr. (2022), respectively.

Relative error (%)	SFM				SFM2				CSM			
	Nucleus		Cell		Nucleus		Cell		Nucleus		Cell	
	a	ϕ	a	ϕ	a	ϕ	a	ϕ	a	ϕ	a	ϕ
<i>fminsearch</i>												
4T1	8	147	39	29	24	31	20	2	42	13	36	19
JC	16	196	47	26	40	49	25	14	50	27	44	9
LMTK	33	227	14	15	14	46	2	6	21	7	21	31
MAT	97	513	14	37	1	47	0	8	31	285	44	68
<i>fmincon</i>												
4T1	14	117	44	38	13	135	39	23	24	19	15	12
JC	25	153	53	37	21	120	43	16	29	14	24	8
LMTK	14	183	27	27	1	207	25	9	11	23	4	8
MAT	59	403	8	13	16	174	9	10	6	22	9	19

Table A1. Relative errors of the mean nucleus and cell radius and volume fraction estimates from CP biophantoms with the log cost function using optical-measured histology as the approximated ground truth for SFM, SFM2 and CSM and with both *fminsearch* (without constraints) and *fmincon* (with constraints) optimization strategies. Results in bold highlight relative errors less than 20%

biophantoms. *The Journal of the Acoustical Society of America* 130(6): 4139–4147.

Han A, Abuhabshah R, Miller RJ, Sarwate S and O'Brien Jr WD (2013) The measurement of ultrasound backscattering from cell pellet biophantoms and tumors ex vivo. *The Journal of the Acoustical Society of America* 134(1): 686–693.

Han A, Zhang YN, Boehringer AS, Montes V, Andre MP, Erdman JW, Loomba R, Valasek MA, Sirlin CB and O'Brien Jr WD (2020) Assessment of Hepatic Steatosis

in Nonalcoholic Fatty Liver Disease by Using Quantitative US. *Radiology* 295(1): 106–113. DOI:10.1148/radiol.2020191152. URL <https://pubs.rsna.org/doi/full/10.1148/radiol.2020191152>. Publisher: Radiological Society of North America.

Insana MF, Brown DG and Shung KK (1993) Acoustic scattering theory applied to soft biological tissues. In: *Ultrasonic scattering in biological tissues*. CRC Press Boca Raton, FL, pp. 75–124.

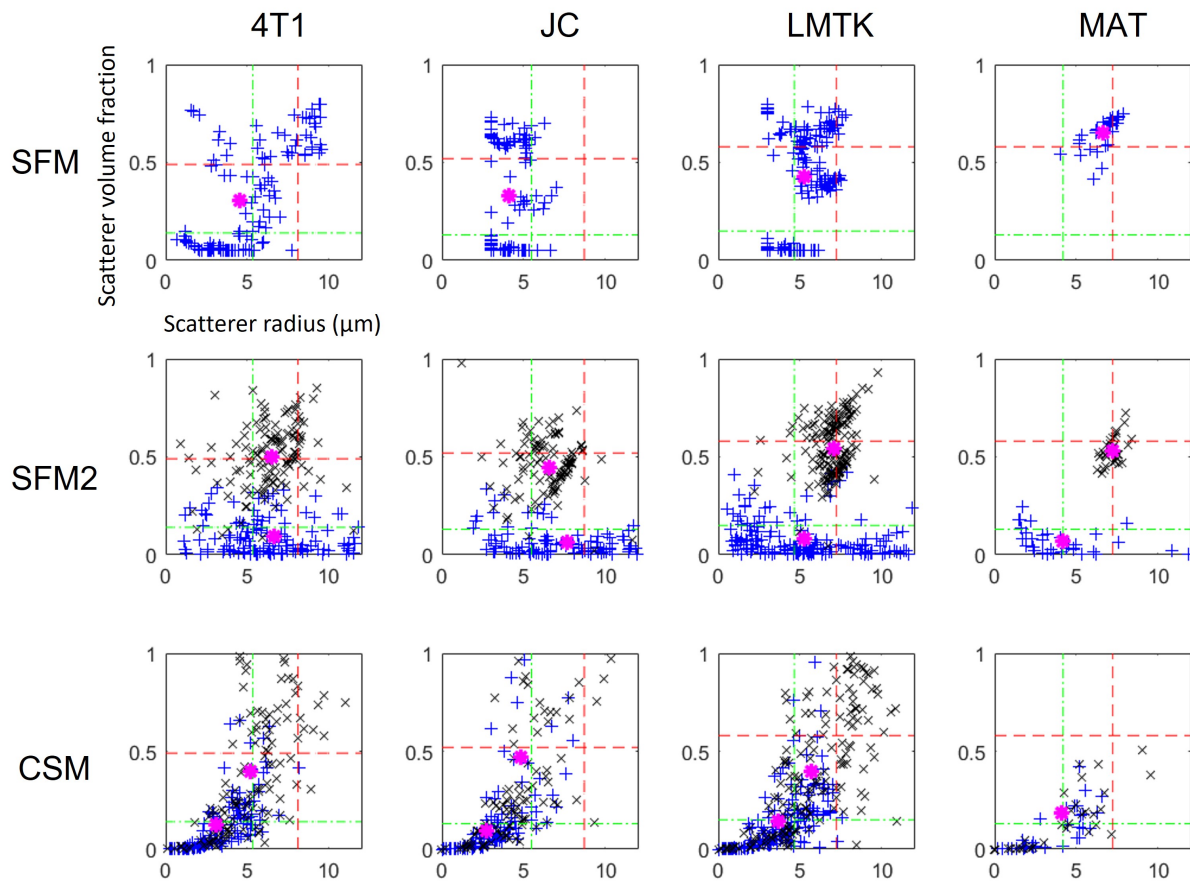


Figure A3. Scatterer radius vs. volume fraction for 4T1 (first row), JC (second row), LMTK (third row) and MAT (fourth row) CP biophantoms obtained with SFM (first line), SFM2 (second line) and CSM (third line) with *fminsearch* optimization strategy using the Log cost function. For SFM2 and CSM, blue +: scatterers correspond to nuclei, and black x: scatterers correspond to cells. The magenta asterisks correspond to the mean value of each distribution. The green (a_N & ϕ_N) and red (a_C & ϕ_C) dashed lines correspond to the mean optical-measured histology nucleus and cell radii and volume fractions from [Muleki-Seya and O'Brien Jr. \(2022\)](#), respectively.

Coefficient of variation	SFM		SFM2				CSM			
			Nucleus		Cell		Nucleus		Cell	
	a	ϕ	a	ϕ	a	ϕ	a	ϕ	a	ϕ
<i>fminsearch</i>										
4T1	0.50	1.05	0.47	0.94	0.30	0.34	0.69	1.24	0.45	0.94
JC	0.49	0.99	0.44	1.04	0.27	0.34	0.91	4.14	0.57	1.97
LMTK	0.40	0.75	0.61	1.19	0.19	0.29	0.54	1.15	0.46	0.79
MAT	0.10	0.16	0.61	0.91	0.07	0.14	1.11	3.75	0.61	1.48
<i>fmincon</i>										
4T1	0.32	0.86	0.35	0.76	0.33	0.19	0.20	0.41	0.16	0.31
JC	0.26	0.80	0.35	0.85	0.33	0.17	0.18	0.62	0.14	0.58
LMTK	0.27	0.61	0.35	0.56	0.30	0.15	0.17	0.38	0.15	0.31
MAT	0.13	0.12	0.39	0.68	0.22	0.12	0.18	0.38	0.15	0.33

Table A2. Coefficients of variation obtained for radius and volume fraction estimates of 4T1, JC, LMTK and MAT CP biophantoms using SFM, SFM2 and CSM for *fminsearch* and *fmincon* optimization strategies with the Log cost function. For SFM2 and CSM, the two coefficients of variation for the radius and the volume fraction correspond to those related to the nucleus and cell estimates.

Kemmerer JP, Ghoshal G, Karunakaran C and Oelze ML (2013) Assessment of high-intensity focused ultrasound treatment of rodent mammary tumors using ultrasound backscatter coefficients. *The Journal of the Acoustical Society of America* 134(2): 1559–1568.

Kolios MC, Czarnota GJ, Lee M, Hunt JW and Sherar MD (2002) Ultrasonic spectral parameter characterization of apoptosis. *Ultrasound in Medicine & Biology* 28(5): 589–597.

Lin SC, Heba E, Wolfson T, Ang B, Gamst A, Han A, Erdman JW, O'Brien Jr WD, Andre MP, Sirlin CB and Loomba R (2015) Noninvasive Diagnosis of Nonalcoholic Fatty Liver Disease and Quantification of Liver Fat Using a New Quantitative Ultrasound Technique. *Clinical Gastroenterology and Hepatology* 13(7): 1337–1345.e6.

Mamou J, Coron A, Oelze ML, Saegusa-Becroft E, Hata M, Lee P, Machi J, Yanagihara E, Laugier P and Feleppa EJ

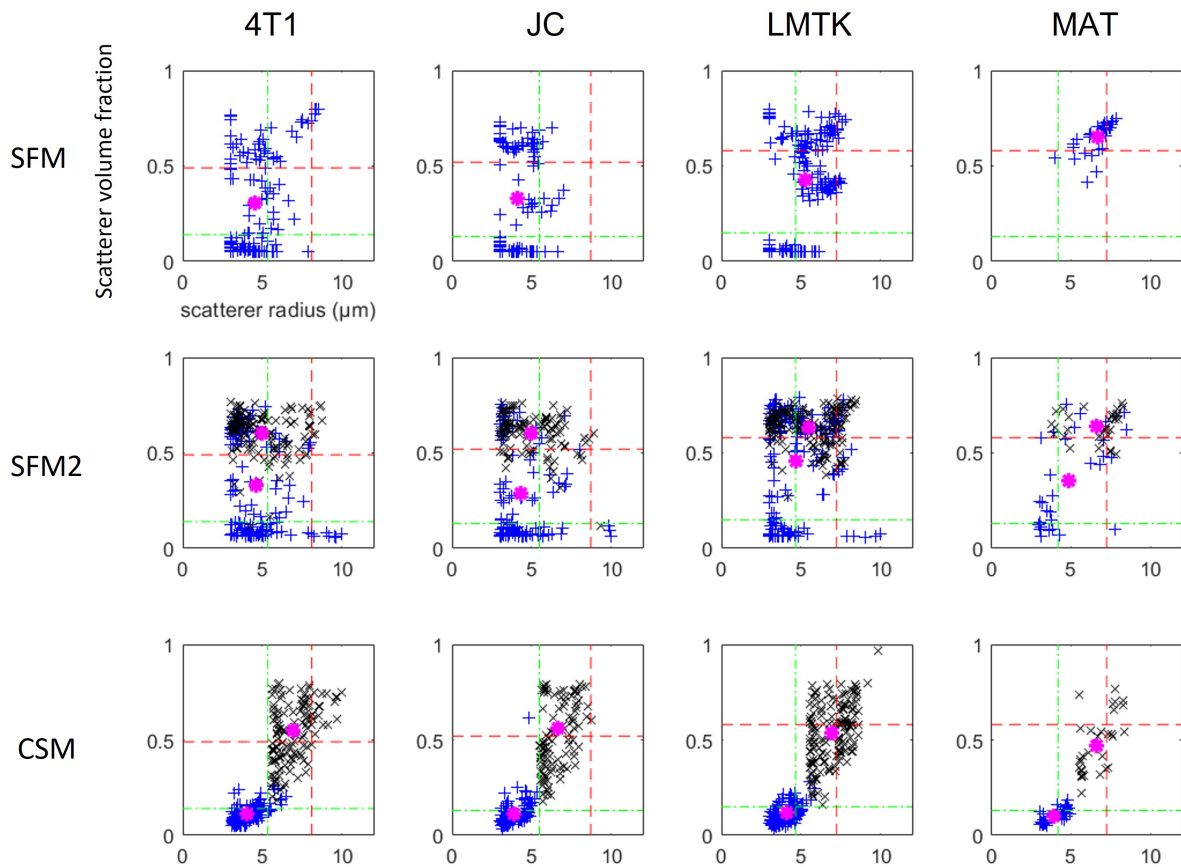


Figure A4. Scatterer radius vs. volume fraction for 4T1 (first row), JC (second row), LMTK (third row) and MAT (fourth row) CP biophantoms obtained with SFM (first line), SFM2 (second line) and CSM (third line) with *fmincon* optimization strategy using the Log cost function. For SFM2 and CSM, blue +: scatterers correspond to nuclei, and black x: scatterers correspond to cells. The magenta asterisks correspond to the mean value of each distribution. The green (a_N & ϕ_N) and red (a_C & ϕ_C) dashed lines correspond to the mean optical-measured histology nucleus and cell radii and volume fractions from Muleki-Seya and O'Brien Jr. (2022), respectively.

Correct (%)	SFM		SFM2			CSM		
<i>fminsearch</i>	N	C	N	C	NC	N	C	NC
4T1	5	0	8	23	2	7	5	1
JC	0	0	1	25	0	5	1	0
LMTK	0	2	2	42	1	6	9	2
MAT	0	6	0	82	0	3	0	0
<i>fmincon</i>								
4T1	2	0	6	8	0	20	19	5
JC	0	0	2	8	0	12	15	5
LMTK	0	14	0	27	0	31	39	22
MAT	0	30	3	52	3	33	30	21

Table A3. Percentage of "correct" nucleus (N) and cell (C) and simultaneous nucleus and cell (NC) estimates using SFM, SFM2 and CSM for 4T1, JC, LMTK and MAT CP biophantoms with both *fminsearch* and *fmincon* optimization strategies and the Log cost function. Results in bold highlight designate when a higher percentage of correct estimates was obtained using *fmincon* instead of *fminsearch*.

(2011) Three-Dimensional High-Frequency Backscatter and Envelope Quantification of Cancerous Human Lymph Nodes. *Ultrasound in Medicine & Biology* 37(3): 345–357.

McNew J, Lavarello R and O'Brien Jr WD (2009) Sound scattering from two concentric fluid spheres. *The Journal of the Acoustical Society of America* 125(1): 1–4.

Muleki-Seya P, Guillermin R, Guglielmi J, Chen J, Pourcher T, Konofagou E and Franceschini E (2016) High-Frequency Quantitative Ultrasound Spectroscopy of Excised Canine Livers and Mouse Tumors Using the Structure Factor

Model. *IEEE Transactions on Ultrasonics, Ferroelectrics, and Frequency Control* 63(9): 1335–1350.

Muleki-Seya P, Han A and O'Brien Jr WD (2022) Evaluation of ultrasound scattering models adapted for two types of scatterers to extract scatterer parameters from cell-pellet biophantoms. In: *2022 IEEE International Ultrasonics Symposium (IUS)*. pp. 1–4. DOI:10.1109/IUS54386.2022.9957992. ISSN: 1948-5727.

Muleki-Seya P and O'Brien Jr WD (2022) Ultrasound Scattering From Cell-Pellet Biophantoms and Ex Vivo Tumors Provides

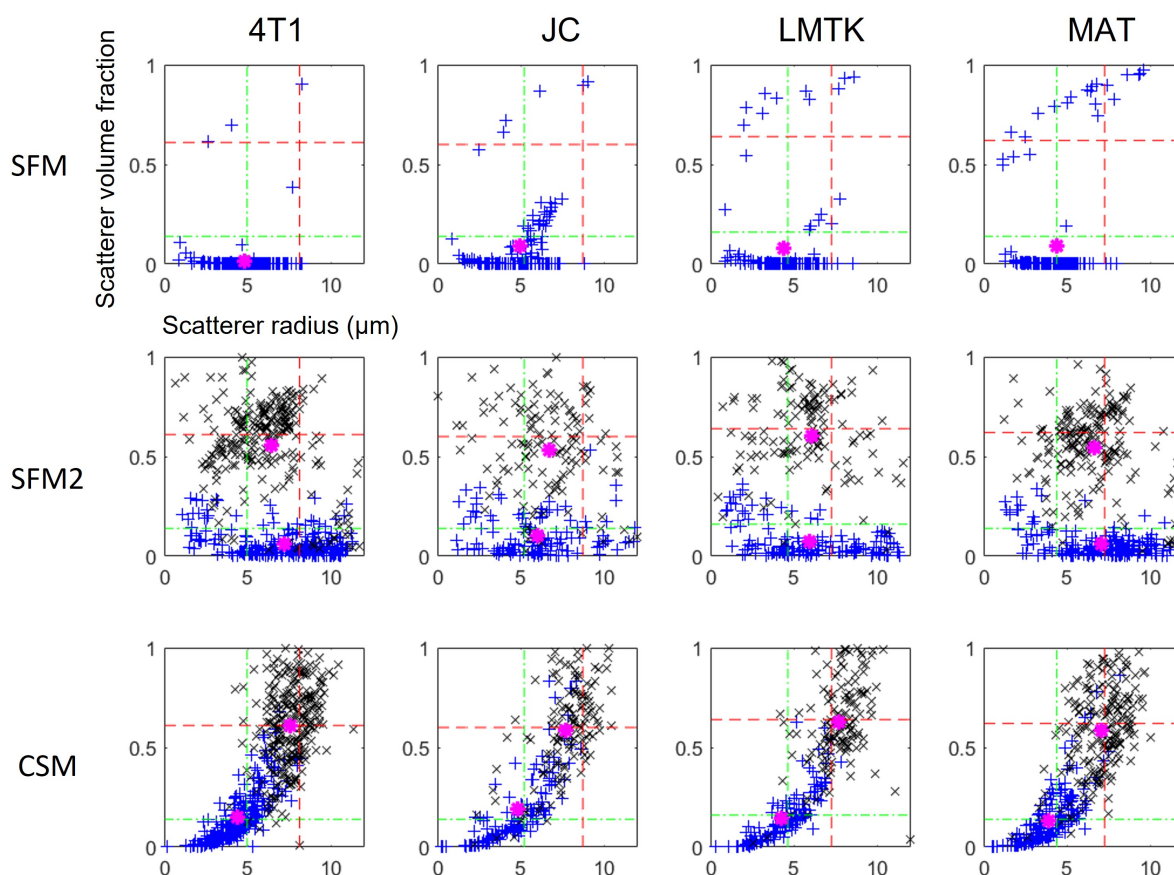


Figure A5. Scatterer radius vs. volume fraction for 4T1 (first row), JC (second row), LMTK (third row) and MAT (fourth row) tumors obtained with SFM (first line), SFM2 (second line) and CSM (third line) with *fminsearch* optimization strategy. For SFM2 and CSM, blue +: scatterers correspond to nuclei, and black x: scatterers correspond to cells. The magenta asterisks correspond to the mean value of each distribution. The green (a_N & ϕ_N) and red (a_C & ϕ_C) dashed lines correspond to the mean optical-measured histology nucleus and cell radii and volume fractions from Muleki-Seya and O'Brien Jr. (2022), respectively.

Insight Into the Cellular Structure Involved in Scattering. *IEEE Transactions on Ultrasonics, Ferroelectrics, and Frequency Control* 69(2): 637–649.

84(1): 52–58.

Oelze ML and O'Brien Jr WD (2006) Application of Three Scattering Models to Characterization of Solid Tumors in Mice. *Ultrasonic Imaging* 28(2): 83–96.

Teisseire M, Han A, Abuhabsah R, Blue JP, Sarwate S and O'Brien Jr WD (2010) Ultrasonic backscatter coefficient quantitative estimates from Chinese hamster ovary cell pellet biophantoms. *The Journal of the Acoustical Society of America* 128(5): 3175–3180.

Twersky V (1987) Low-frequency scattering by correlated distributions of randomly oriented particles. *The Journal of the Acoustical Society of America* 81(5): 1609–1618.

Wertheim MS (1963) Exact Solution of the Percus-Yevick Integral Equation for Hard Spheres. *Physical Review Letters* 10(8): 321–323.

Wu Y, Lopez L, Andre MP, Loomba R, Sirlin CB, Valasek MA, Wallig MA, O'Brien WDJ and Han A (2020) Liver Fat Droplet Dependency on Ultrasound Backscatter Coefficient in Nonalcoholic Fatty Liver. In: *2020 IEEE International Ultrasonics Symposium (IUS)*. pp. 1–4. DOI:10.1109/IUS46767.2020.9251748. ISSN: 1948-5727.

Yuan YW and Shung KK (1988) Ultrasonic backscatter from flowing whole blood. I: Dependence on shear rate and hematocrit. *The Journal of the Acoustical Society of America*

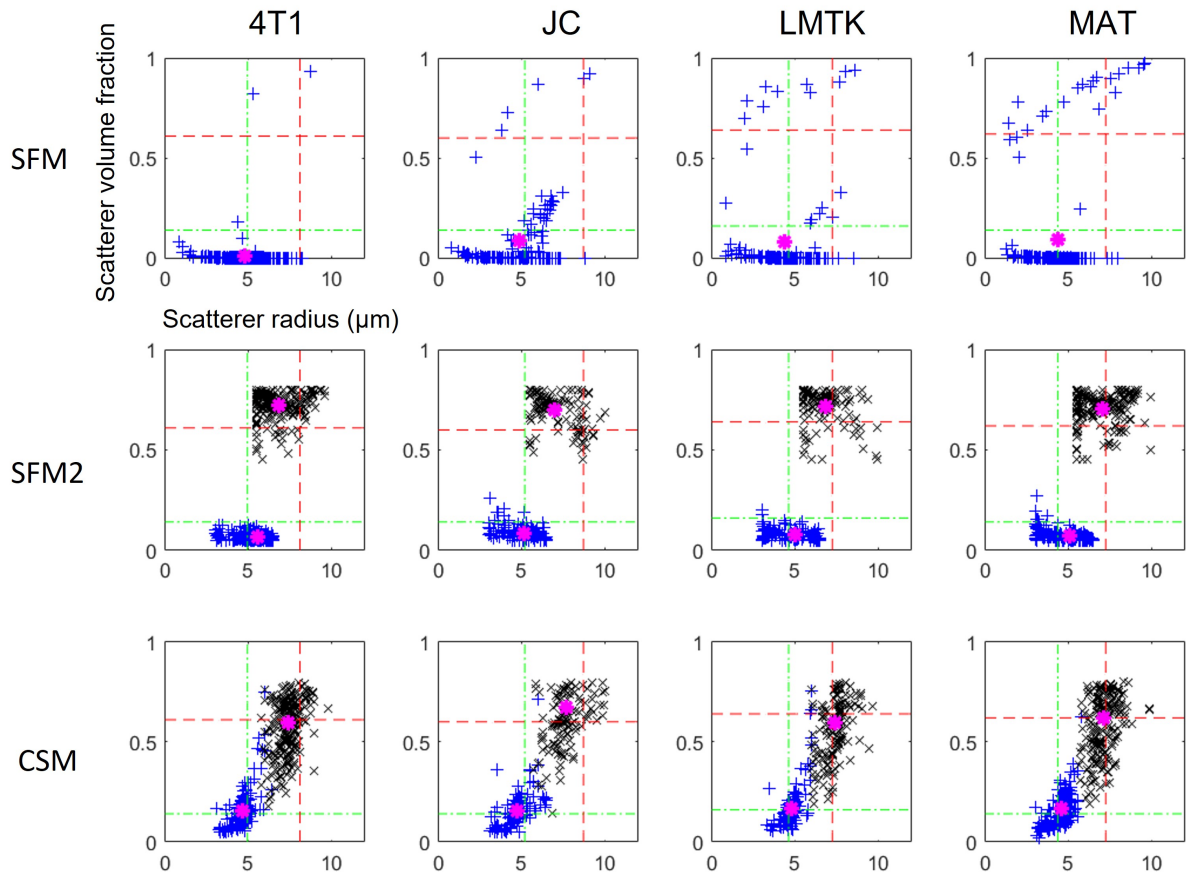


Figure A6. Scatterer radius vs. volume fraction for 4T1 (first row), JC (second row), LMTK (third row) and MAT (fourth row) tumors obtained with SFM (first line), SFM2 (second line) and CSM (third line) with *fmincon* optimization strategy. For SFM2 and CSM, blue +: scatterers correspond to nuclei, and black x: scatterers correspond to cells. The magenta asterisks correspond to the mean value of each distribution. The green (a_N & ϕ_N) and red (a_C & ϕ_C) dashed lines correspond to the mean optical-measured histology nucleus and cell radii and volume fractions from [Muleki-Seya and O'Brien Jr. \(2022\)](#), respectively.